PUBLICATIONS OF THE ASTRONOMICAL SOCIETY OF THE PACIFIC, **113**:1365–1377, 2001 November

Lick Spectral Indices for Super–Metal-rich Stars[1]

A. BUZZONI

Telescopio Nazionale Galileo, A.P. 565, E-38700 Santa Cruz de La Palma, Canary Islands, Spain;
and Osservatorio Astronomico di Brera, Milano, Italy; buzzoni@tng.iac.es

M. CHAVEZ

Instituto Nacional de Astrofísica, Optica y Electrónica, A.P. 51 y 216, 72000 Puebla, Mexico; mchavez@inaoep.mx

M. L. MALAGNINI

Dipartimento di Astronomia, Università di Trieste, Via G. B. Tiepolo 11, I-34131 Trieste, Italy; malagnini@ts.astro.it

AND

C. MOROSSI

Osservatorio Astronomico di Trieste, Via G. B. Tiepolo 11, I-34131 Trieste, Italy; morossi@ts.astro.it

Received 2001 June 12; accepted 2001 July 25

ABSTRACT. We present Lick spectral indices for a complete sample of 139 candidate super–metal-rich stars of different luminosity classes (MK type from I to V). For 91 of these stars we were able to identify, in an accompanying paper, the fundamental atmosphere parameters. This confirms that at least 2/3 of the sample consists of stars with [Fe/H] in excess of +0.1 dex. Optical indices for both observations and fiducial synthetic spectra have been calibrated to the Lick system according to Worthey et al. and include the Fe I indices of Fe5015, Fe5270, and Fe5335 and the Mg I and MgH indices of Mg_2 and Mg *b* at 5180 Å. The internal accuracy of the observations is found to be σ(Fe5015) = ±0.32 Å, σ(Fe5270) = ±0.19 Å, σ(Fe5335) = ±0.22 Å, $\sigma(Mg_2)$ = ±0.004 mag, and σ(Mg *b*) = ±0.19 Å. This is about a factor of 2 better than the corresponding theoretical indices from the synthetic spectra, the latter being a consequence of the intrinsic limitations in the input physics, as discussed by Chavez et al.

By comparing models and observations, we find no evidence for nonstandard Mg versus Fe relative abundance, so [Mg/Fe] = 0, on the average, for our sample. Both the Worthey et al. and Buzzoni et al. fitting functions are found to suitably match the data and can therefore confidently be extended for population synthesis application also to supersolar metallicity regimes. A somewhat different behavior of the two fitting sets appears, however, beyond the temperature constraints of our stellar sample. Its impact on the theoretical output is discussed, as far as the integrated Mg_2 index is derived from synthesis models of stellar aggregates. A two-index plot, such as Mg_2 versus Fe5270, is found to provide a simple and powerful tool for probing distinctive properties of single stars and stellar aggregates as a whole. The major advantage, over a classical CM diagram, is that it is both reddening free and distance independent.

1. INTRODUCTION

A fair recognition of super–metal-rich (SMR) stars in the solar neighborhood remains a crucial issue to resolve before we can confidently assess the problem of a metallicity estimate in the Galaxy bulge and external galaxies, via population synthesis models.

In the classical works on the subject (Spinrad & Taylor 1969), the definition of SMR candidates mostly relied on the relative chemical abundance with respect to the Hyades and set the nominal threshold for SMR stars at [Fe/H] > +0.2 dex (i.e., a metal abundance *Z* in excess of 50% over the solar abundance).

Both the metallicity scale for the bulge stellar population (Frogel 1999) as well as the individual estimates of *Z* for the most metal-rich template stars in the disk (first of all the classical SMR standard μ Leo; see McWilliam 1997; Taylor 1999; Smith & Ruck 2000) have however been the subject of important revisions in the recent literature, although no conclusive argument seems so far to definitely settle the problem.

In this paper, we follow on the spectroscopic study of a sample of SMR candidates undertaken in Malagnini et al. (2000, hereafter Paper I), providing a detailed calibration for the main Lick narrowband indices in the optical wavelength

[1] Based on observations collected at the Instituto Nacional de Astrofísica, Optica y Electrónica (INAOE) "G. Haro" Observatory, Cananea (Mexico).

range. These include the two Mg indices (Mg_2 and Mg *b*) and the three Fe I indices Fe5015, Fe5270, and Fe5335 (hereafter Fe50, Fe52, and Fe53, respectively; see § 2).

For most of these stars, we identified in Paper I the photospheric *fiducial* parameters ($T_{\rm eff}$, $\log g$, and [M/H]) and computed the corresponding synthetic spectra according to the Chavez, Malagnini, & Morossi (1997) theoretical database. Theoretical narrowband indices will be especially dealt with in § 3, where we address the problem of a possible nonsolar [Mg/Fe] chemical partition of our SMR candidates.

A metallicity estimate in external galaxies should forcedly rely on population synthesis models by matching integrated indices for the whole stellar aggregate. This is usually done by means of the so-called fitting function technique (Worthey et al. 1994, hereafter W94; Buzzoni, Gariboldi, & Mantegazza 1992, hereafter B92; and Buzzoni, Mantegazza, & Gariboldi 1994, hereafter B94), that is, by fitting index behavior for local stars and implementing this analytical framework in the synthesis code. It is of paramount importance, in this sense, to confidently validate fitting function predictions also to supersolar metallicity regimes. This is done in § 4, where we check our observations against the W94, B92, and B94 fitting sets.

The Mg_2 versus Fe52 plot could reveal a simple and powerful tool for stellar diagnostics for both individual objects and stellar aggregates. Its major advantage over the classical CM diagrams is that it is both reddening free and distance independent. In § 5 we will discuss in some detail its possible applications by referring to our stellar sample.

2. OBSERVATIONS AND SYSTEM CALIBRATION

The original set of observations of this work consists of 139 bright stars ($V < 8$ mag) in the spectral range between F and M and luminosity class between I and V, selected from three main reference sources for metallicity in the literature.

Dwarf stars (classes IV–V) mainly come from the general catalog of Cayrel de Strobel et al. (1997), while giants (classes I–III) are mostly from Taylor (1991). These two data sources were then completed with the work of W94 in order to include a set of primary calibrators to the Lick system and provide a more homogeneous distribution among all luminosity classes.

Each of our SMR candidates is quoted to have *at least* one determination of [Fe/H] $\geq +0.1$ from high-resolution abundance studies in the literature.

This working sample was observed during three runs, between 1995 December and 1996 August, at the 2.12 m f/12 telescope of the INAOE "G. Haro" Observatory in Cananea (Mexico). We collected Böller & Chivens mid-dispersion (35 Å mm^{-1}) spectra at $R = \lambda/\Delta\lambda = 2000$ inverse resolution (namely, some 2.5 Å FWHM) in the wavelength range between 4600 and 5500 Å. Full details of the observing setup as well as of the data reduction can be found in Paper I.

A total of 100 stars had two or more observations on different nights, while 39 stars were observed only once. Typically, a pixel-to-pixel signal-to-noise ratio (S/N) greater than 50 was achieved in the 250 observed spectra.

Wavelength calibration eventually provided a ± 0.09 Å accuracy, while the spectral energy distribution (SED) of stars was obtained within a $\pm 10\%$ relative flux level. Flux rebinning to a fixed $\Delta\lambda$/pixel ratio was performed, preserving the total number of pixels as in the original observations.

Multiple observations also allowed us an independent estimate of the internal uncertainty of the whole data set. They confirmed in particular a pixel-to-pixel photon noise better than ± 0.02 mag, in agreement with the observed S/N ratio, with the only relevant exception being star HD 36389, which had poorer observations and S/N = 6 (see Table 1 in Paper I). Repeated observations for each star were eventually co-added after calibration in order to obtain one mean spectrum for each object.

Table 1 reports a full summary of the observed stellar sample, listing in columns (1)–(4) the HD number, spectral type, number of collected spectra, and mean flux uncertainty as from the standard deviation of the relative flux for repeated observations, respectively.[2]

2.1. Matching the Lick System

Three striking features of Fe I and the atomic-molecular blend of Mg I and MgH are present in the wavelength range of our spectra.

Each of these features has been included in the narrowband spectral indices of the Lick system (Faber, Burstein, & Dressler 1977), in its recent extension by W94. A measure of the line strength is provided in this system by interpolating a local continuum (f_c) from two sidebands adjacent to each relevant feature and evaluating therefrom a pseudo–equivalent width (EW) such as

$$\begin{aligned} \mathrm{EW} &= \int \{[\, f_c(\lambda) - f(\lambda)]/f_c(\lambda)\}\, d\lambda \\ &= \Delta\lambda_f (1 - \langle f/f_c \rangle), \end{aligned} \tag{1}$$

where $\Delta\lambda_f$ is the width of the spectral window centered on the absorption feature.

For some molecular blends, it is useful to define an index in magnitude scale ($I_{\rm mag}$) so that

$$\begin{aligned} I_{\rm mag} &= -2.5 \log \left\{ \int [\, f(\lambda)/f_c(\lambda)] d\lambda/\Delta\lambda_f \right\} \\ &= -2.5 \log \langle f/f_c \rangle. \end{aligned} \tag{2}$$

Both formalisms are however equivalent (see also Brodie &

[2] For single observations, a mean σ(flux) = 0.02 will be assumed in this work.

TABLE 1
OBSERVATIONAL DATABASE AND STANDARD LICK INDICES

Source (HD) (1)	Spectral Type (2)	n(obs) (3)	σ(flux) (4)	Fe50 (Å) (5)	Mg_2 (mag) (6)	Mg b (Å) (7)	Fe52 (Å) (8)	Fe53 (Å) (9)	[Fe/H][a] (10)	Remarks[b] (11)
4	F0	1	…	4.098	0.075	1.447	1.682	1.269	+0.3	
1461	G0 V	2	0.0048	4.552	0.148	3.175	2.487	1.932	+0.43	W
1835	G3 V	2	0.0109	4.722	0.148	3.019	2.515	1.968	+0.19	B
4188	K0 III	3	0.0068	5.952	0.105	2.548	3.096	2.491	−0.16	
6497	K2 III	3	0.0061	6.294	0.307	4.131	3.736	3.351	…	
8673	F7 V	2	0.0037	3.754	0.085	1.505	1.574	1.233	+0.16	
10307	G1.5 V	3	0.0068	3.766	0.136	2.610	2.160	1.565	−0.02	W
10780	K0 V	2	0.0046	4.690	0.228	4.677	3.026	2.441	+0.36	W
15152	K5 III	2	0.0095	7.602	0.437	4.389	4.366	4.385	…	
16232	F6 V	2	0.0051	3.284	0.062	1.119	1.408	0.984	+0.27	
17017	K2 III	2	0.0076	6.399	0.252	3.513	3.621	3.149	…	
18322	K1 III	2	0.0056	5.838	0.201	3.197	3.353	2.788	−0.23	B
19476	K0 III	4	0.0068	6.080	0.184	2.826	3.312	2.749	+0.04	W
20630	G5 V	2	0.0080	4.245	0.155	3.049	2.460	1.912	−0.01	W, B
20675	F6 V	3	0.0047	3.725	0.065	1.079	1.485	1.170	+0.2	
21488	K0	4	0.0159	5.023	0.162	2.164	2.574	2.276	…	
24240	K0 III	3	0.0065	6.730	0.176	2.597	3.423	2.894	…	
24802	K0	3	0.0081	7.159	0.250	2.782	3.949	3.396	…	
25975	K1 III	3	0.0052	5.416	0.224	3.772	3.261	2.681	…	
26462	F4 V	3	0.0016	3.142	0.060	0.901	1.278	0.965	…	W
26846	K3 III	2	0.0041	6.741	0.267	3.843	3.758	3.352	+0.21	
27371	K0 III	3	0.0060	6.333	0.169	2.459	3.228	2.703	−0.02	W
27697	K0 I	3	0.0017	6.349	0.177	2.434	3.251	2.699	…	W
28307	K0 IIIb	3	0.0019	6.124	0.185	2.637	3.148	2.654	…	W
30495	G3 V	2	0.0026	3.932	0.121	2.857	2.181	1.676	+0.1	B
30562	F8 V	2	0.0032	4.708	0.121	2.390	2.229	1.774	+0.14	B
30652	F6 V	3	0.0039	3.341	0.075	1.326	1.445	1.101	+0.02	W
32068	K4 Ib–II+	2	0.0101	8.411	0.350	3.018	4.563	4.453	+0.1	
32393	K3	1	…	7.057	0.328	4.093	4.063	3.702	…	
33276	F2 IV	2	0.0076	3.342	0.064	0.989	1.381	1.116	+0.29	
34411	G1.5 IV–V	2	0.0034	4.212	0.122	2.523	2.057	1.661	+0.06	W
35620	K3 IIICN+	1	…	7.232	0.360	3.721	4.262	4.046	−0.09	W
36040	K0 IIIp	1	…	6.828	0.242	3.321	3.650	3.134	…	
36389	M2 Iab	2	0.0066	7.183	0.232	2.889	2.977	3.005	+0.11	
37387	K1 Ib	1	…	10.895	0.250	1.484	4.831	4.433	+0.13	
37763	K3 III	1	…	7.135	0.329	4.119	4.068	3.742	+0.3	B
42341	K2 III	1	…	7.144	0.294	4.154	3.980	3.670	…	
44391	K0 Ib	2	0.0111	8.916	0.164	1.373	3.919	3.278	+0.21	
44478	M3 II	2	0.0095	10.685	0.491	7.131	3.563	3.502	…	
45412	F8 Ib var	2	0.0046	5.721	0.062	0.187	2.048	1.682	+0.1	
46709	K4 III	2	0.0101	7.900	0.359	3.444	4.492	4.297	…	
47174	K3 Iab:	2	0.0046	6.988	0.237	2.958	3.766	3.226	…	
48682	G0 V	2	0.0083	3.972	0.092	2.106	1.845	1.475	+0.15	W
49161	K4 III	2	0.0052	7.931	0.344	3.709	4.353	4.248	…	W
52973	G0 Ib var	2	0.0078	7.722	0.096	0.258	2.745	2.083	+0.49	
54719	K2 III	2	0.0071	7.511	0.267	3.405	4.065	3.577	…	W
56577	K4 III	1	…	9.760	0.392	3.437	4.853	4.814	+0.15	B
57727	G8 III	2	0.0045	5.175	0.163	2.536	2.833	2.189	…	
58207	G9 IIIb	2	0.0064	5.832	0.180	2.600	3.057	2.534	−0.17	W
59881	F0 III	3	0.0077	2.642	0.045	0.727	1.115	0.864	+0.19	
60522	M0 I	2	0.0331	5.268	0.451	5.010	4.220	2.926	…	W
61064	F6 III	2	0.0107	4.308	0.060	0.761	1.602	1.259	+0.44	
62902	K5 III	2	0.0091	7.668	0.419	4.766	4.445	4.531	…	
63302	K3 Iab/Ib	1	…	13.493	0.268	0.804	5.656	4.952	+0.17	B
63700	G3 Ib	1	…	10.381	0.140	0.341	4.049	3.527	+0.24	
65714	gG8	2	0.0100	6.773	0.163	2.299	3.288	2.735	…	
72184	K2 III	2	0.0042	6.613	0.278	4.028	3.813	3.322	…	W
72324	G9 I	2	0.0070	6.246	0.168	2.348	3.150	2.544	…	W
72505	K0 III	2	0.0085	6.849	0.300	3.852	3.837	3.455	…	

TABLE 1—*Continued*

Source (HD) (1)	Spectral Type (2)	*n*(obs) (3)	σ(flux) (4)	Fe50 (Å) (5)	Mg_2 (mag) (6)	Mg *b* (Å) (7)	Fe52 (Å) (8)	Fe53 (Å) (9)	[Fe/H][a] (10)	Remarks[b] (11)
72561	G5 III	2	0.0068	6.801	0.145	1.573	3.203	2.583	…	
73665	K0 I	2	0.0071	6.672	0.166	2.382	3.256	2.685	…	W
73710	K0 I	2	0.0303	4.822	0.117	1.399	2.407	1.876	…	W
74739	G7.5 IIIa	2	0.0117	6.479	0.145	1.722	3.038	2.454	−0.14	
75732	G8 V	3	0.0059	5.980	0.309	5.522	3.674	3.089	+0.24	W
78249	K1 IV	2	0.0121	5.558	0.269	4.354	3.427	2.841	…	
81029	F0	1	…	3.298	0.051	0.565	1.515	1.015	+0.27	
81873	K0 III	2	0.0068	6.245	0.199	2.893	3.357	2.806	…	
82734	K0 IV	1	…	6.718	0.168	2.412	3.411	2.908	+0.4	
83951	F3 V	2	0.0045	3.130	0.044	0.853	1.299	0.975	+0.14	
85503	K0 III	2	0.0080	7.532	0.332	4.286	4.135	3.817	−0.01	W
87822	F4 V	2	0.0087	3.489	0.063	1.210	1.491	1.165	+0.19	
88230	K8 V	2	0.0137	5.126	0.527	4.759	4.442	4.106	+0.28	W
88284	K0 III	1	…	6.452	0.192	3.049	3.478	2.963	+0.09	W, B
90277	F0 V	2	0.0082	3.129	0.046	0.739	1.297	0.960	+0.19	
92125	G2.5 IIa	2	0.0129	6.431	0.106	1.088	2.515	2.168	−0.24	
93257	gK3	2	0.0139	6.408	0.303	4.284	3.796	3.337	…	
95272	K0 III	1	…	6.216	0.206	2.965	3.397	2.818	−0.22	W, B
95849	K3 III	2	0.0106	7.243	0.270	3.560	3.909	3.559	…	
100563	F5 V	2	0.0087	3.488	0.066	1.418	1.489	1.203	+0.12	
101013	K0 IIIp	1	…	5.099	0.181	1.888	2.809	1.980	…	
102328	K3 III	2	0.0171	7.468	0.365	4.487	4.216	4.019	…	W
102634	F7 V	2	0.0055	4.060	0.085	1.782	1.798	1.373	+0.1	B
102870	F9 V	2	0.0044	4.127	0.084	1.814	1.876	1.429	+0.18	W, B
104304	G9 IV	2	0.0045	5.174	0.213	4.120	2.989	2.400	+0.18	
109511	K2 III	2	0.0089	6.663	0.206	2.834	3.603	3.057	−0.09	
110014	K2 III	1	…	7.518	0.294	3.617	4.252	3.769	…	
113022	F6 Vs	1	…	3.576	0.057	1.432	1.500	1.109	+0.1	
114710	F9.5 V	1	…	3.775	0.088	2.282	1.880	1.450	+0.02	W
115604	F3 III	1	…	4.506	0.057	0.693	1.713	1.373	+0.18	
120136	F6 IV	1	…	3.940	0.058	1.544	1.750	1.326	+0.14	W
121370	G0 IV	1	…	4.704	0.077	1.700	2.022	1.585	+0.16	W
124425	F7 IV	1	…	3.587	0.047	1.010	1.496	1.044	…	
124570	F6 IV	1	…	3.952	0.069	1.517	1.702	1.325	+0.12	
125560	K3 III	1	…	7.148	0.316	4.028	4.080	3.695	…	W
127227	K5 III	1	…	7.608	0.464	4.680	4.275	4.491	…	
129989	K0 II–III	1	…	7.623	0.160	2.054	3.549	3.004	−0.13	
130948	G1 V	1	…	3.712	0.113	2.327	1.886	1.413	+0.2	
136028	K5 I	1	…	4.126	0.341	4.093	4.156	2.102	…	W
139357	gK4	1	…	7.535	0.268	3.807	4.010	3.709	…	
140573	K2 IIIb	1	…	7.236	0.256	3.693	3.898	3.548	+0.23	W
144284	F8 IV	4	0.0063	4.098	0.075	1.447	1.682	1.269	+0.2	
145000	K1 III	1	…	6.841	0.224	3.366	3.649	3.219	…	
145675	K0 V	2	0.0101	6.036	0.292	5.508	3.640	3.158	+0.18	W
146051	M0.5 III	2	0.0093	7.362	0.447	4.757	3.818	3.970	+0.32	
147677	K0 III	1	…	6.039	0.158	2.633	3.195	2.651	…	W
148513	K4 III	1	…	7.460	0.369	3.948	4.312	4.276	…	W
150680	G0 IV	2	0.0055	4.390	0.101	2.022	2.030	1.636	−0.07	
153956	gK1	1	…	6.821	0.276	3.564	3.812	3.324	…	
156266	K2 III	1	…	6.692	0.252	3.512	3.830	3.320	…	
156283	K3 Iab:	2	0.0100	7.798	0.310	3.083	4.250	3.899	−0.18	
157881	K7 V	2	0.0067	5.017	0.517	4.687	4.419	4.156	+0.4	
159181	G2 Iab:	2	0.0075	7.377	0.107	0.735	2.763	2.394	+0.14	
159925	G9 III	1	…	6.117	0.137	2.129	3.123	2.432	…	
160922	F5 V	2	0.0091	3.211	0.058	1.323	1.423	1.054	+0.4	
161096	K2 III	2	0.0146	7.130	0.271	3.866	3.824	3.494	+0.14	
161797	G5 IV	3	0.0053	5.166	0.161	3.128	2.641	2.112	+0.16	W

TABLE 1—*Continued*

Source (HD) (1)	Spectral Type (2)	n(obs) (3)	σ(flux) (4)	Fe50 (Å) (5)	Mg_2 (mag) (6)	Mg b (Å) (7)	Fe52 (Å) (8)	Fe53 (Å) (9)	[Fe/H][a] (10)	Remarks[b] (11)
162917	F4 IV–V	4	0.0049	3.343	0.055	1.241	1.302	0.865	+0.1	
163770	K1 IIaCN+	1	…	9.177	0.208	1.748	4.253	3.827	−0.24	
163993	G8 III	3	0.0056	5.796	0.149	2.498	2.928	2.342	−0.1	
166229	K2.5 III	1	…	6.535	0.283	3.936	3.798	3.386	…	
167858	F2 V	3	0.0067	2.805	0.029	0.792	1.137	0.826	+0.17	
171802	F5 III	2	0.0032	2.949	0.054	1.151	1.259	0.772	+0.1	
181276	G9 III	2	0.0055	5.863	0.162	2.696	2.990	2.284	−0.08	
182572	G8 IV	2	0.0040	5.408	0.200	3.788	2.787	2.271	+0.15	W
186408	G1 V	2	0.0043	4.281	0.129	2.931	2.085	1.604	+0.06	W
187238	K3 Ia0–Ia	3	0.0054	10.377	0.324	2.424	4.690	4.407	+0.2	
187299	G5 Ia0–Ib	2	0.0054	9.634	0.186	1.179	3.954	3.374	+0.16	
187691	F8 V	2	0.0037	3.958	0.091	1.987	1.714	1.285	+0.09	W
187921	G2.5: Iab	3	0.0101	10.689	0.136	−0.425	3.711	2.975	+0.28	
196725	K3 Iab	2	0.0070	9.088	0.275	2.517	4.311	4.142	+0.22	
197039	F5	2	0.0034	3.926	0.075	1.465	1.607	1.164	+0.15	
197572	F7 Ib	3	0.0057	8.352	0.105	0.417	2.804	2.215	+0.15	
197963	F7 V	1	…	5.464	0.182	3.030	2.886	2.516	…	
198084	F8 IV–V	2	0.0032	4.106	0.084	1.739	1.727	1.388	+0.12	
201078	F7.5 Ib–IIvar	2	0.0039	4.803	0.057	0.406	1.735	1.203	+0.13	
205512	K0.5 III	2	0.0050	6.232	0.209	3.091	3.262	2.793	+0.2	
209750	G2 Ib	2	0.0049	8.247	0.105	0.531	2.920	2.462	+0.14	
216228	K0 III	2	0.0041	6.104	0.185	2.908	3.136	2.626	+0.09	
221148	K3 IIIvar	2	0.0059	6.925	0.358	5.316	3.909	3.628	+0.09	W, B

[a] From Paper I.

[b] Index calibrator in common with Worthey et al. 1994 (W) or Buzzoni et al. 1992, 1994 (B).

Huchra 1990) as

$$\mathrm{EW} = \Delta\lambda_f(1 - 10^{-0.4I_{\mathrm{mag}}}). \quad (3)$$

For each star in our sample, the Lick indices of Fe50, Fe52, Fe53, Mg_2, and Mg b have been computed in the instrumental system, following W94.

To account for the different spectral resolution of our observations, calibration to the standard system has been accomplished by matching the index calibrators in common with W94, B92, and B94, using the latter ones as a "check sample" in our fit.

We especially confined our analysis to stars of classes III, IV, and V, since class I–II supergiants are often variable stars and are therefore less confident calibrators.

A total of 36 stars were found in common with W94, with all available indices,[3] while 13 secondary calibrators appeared in the B92 and B94 sample with standard Mg_2, Fe52, and Fe53 index measurements.

A zero-average $(O - C)$ residual distribution (in the sense [observed − standard]) was eventually obtained with the following set of transformation equations:

$$\begin{aligned}
(O - C)_{\mathrm{Fe50}} &= 0.139\ \mathrm{Fe50} - 0.278 \quad (\text{Å}) \\
(O - C)_{\mathrm{Mg2}} &= -0.056\ \mathrm{Mg_2} + 0.007 \quad (\text{mag}) \\
(O - C)_{\mathrm{Mg}\,b} &= 0.047\ \mathrm{Mg}\ b - 0.092 \quad (\text{Å}) \\
(O - C)_{\mathrm{Fe52}} &= 0.150\ \mathrm{Fe52} - 0.183 \quad (\text{Å}) \\
(O - C)_{\mathrm{Fe53}} &= 0.163\ \mathrm{Fe53} + 0.078 \quad (\text{Å}). \quad (4)
\end{aligned}$$

In the equations, the input indices are the observed ones (i.e., in the instrumental system). After calibration, the residual standard deviation for the W94 primary calibrators and the B92/B94 "check sample" resulted in

$$\begin{aligned}
\sigma(\mathrm{Fe50}) &= \pm 0.39\ \text{Å} \quad 35\ \text{stars}, \\
\sigma(\mathrm{Mg_2}) &= \pm 0.012\ \text{mag} \quad 49\ \text{stars}, \\
\sigma(\mathrm{Mg}\ b) &= \pm 0.19\ \text{Å} \quad 36\ \text{stars}, \\
\sigma(\mathrm{Fe52}) &= \pm 0.24\ \text{Å} \quad 49\ \text{stars}, \\
\sigma(\mathrm{Fe53}) &= \pm 0.25\ \text{Å} \quad 49\ \text{stars}. \quad (5)
\end{aligned}$$

[3] Apart from HD 49161, which lacks Fe50 in the W94 sample.

Figure 1 summarizes our results, while the complete list of standard indices is reported in columns (5)–(9) of Table 1. When available from Paper I, column (10) provides the fiducial metallicity, while column (11) marks the reference calibrators in common with W94, B92, and B94.

A convenient estimate of the internal uncertainty of the whole data sample can easily derive from the typical pixel-to-pixel S/N ratio, when we recall that $\sigma(\mathrm{flux}) = (\mathrm{S/N})^{-1}$ mag. For each index, therefore, in a magnitude scale we could write

$$\sigma_I = \frac{\sigma(\mathrm{flux})}{\sqrt{N_{\mathrm{red}} + N_{\mathrm{blue}}} + \sqrt{N_{\mathrm{feat}}}}\,(\mathrm{mag}), \tag{6}$$

where N_{red}, N_{blue}, and N_{feat} are the number of pixels in the red and blue continuum sidebands and in the feature window, respectively. To translate from magnitudes to angstrom equivalent width, we simply have

$$\sigma\ (\text{Å}) = \sigma\ (\mathrm{mag}) \times \Delta\lambda_f. \tag{7}$$

The typical internal error bar of our data eventually resulted in

$$\begin{aligned} \sigma(\mathrm{Fe50}) &= \pm 0.32\ \text{Å}, \\ \sigma(\mathrm{Mg_2}) &= \pm 0.004\ \mathrm{mag}, \\ \sigma(\mathrm{Mg}\ b) &= \pm 0.19\ \text{Å}, \\ \sigma(\mathrm{Fe52}) &= \pm 0.19\ \text{Å}, \\ \sigma(\mathrm{Fe53}) &= \pm 0.22\ \text{Å}. \end{aligned} \tag{8}$$

Note that the latter quantities consistently compare with the point scatter of equation (5). This confirms that no residual variance was left in the data after transformation to the standard system via equation (4).

3. THE FIDUCIAL SYNTHETIC SPECTRA

For 73 of the stars in Table 1 (nearly all those of luminosity classes III–V), we identified in Paper I a best choice for the atmosphere fundamental parameters available from high-resolution studies in the literature. In the following, this will be referred to as a "fair" sample. A further subsample of 18 stars had a formal atmosphere solution in our work, but with lower statistical confidence. The total of 91 stars will compose our "extended" sample.

Operationally, in Paper I our strategy was to compute, for each high-resolution parameter set, the corresponding synthetic spectrum from the Chavez et al. (1997) database and pick up the better fit to our mid-resolution spectra. This procedure allowed us to assess physical self-consistency of the high-resolution outputs and provide the best values for $\log T_{\mathrm{eff}}$, $\log g$, and [Fe/H].

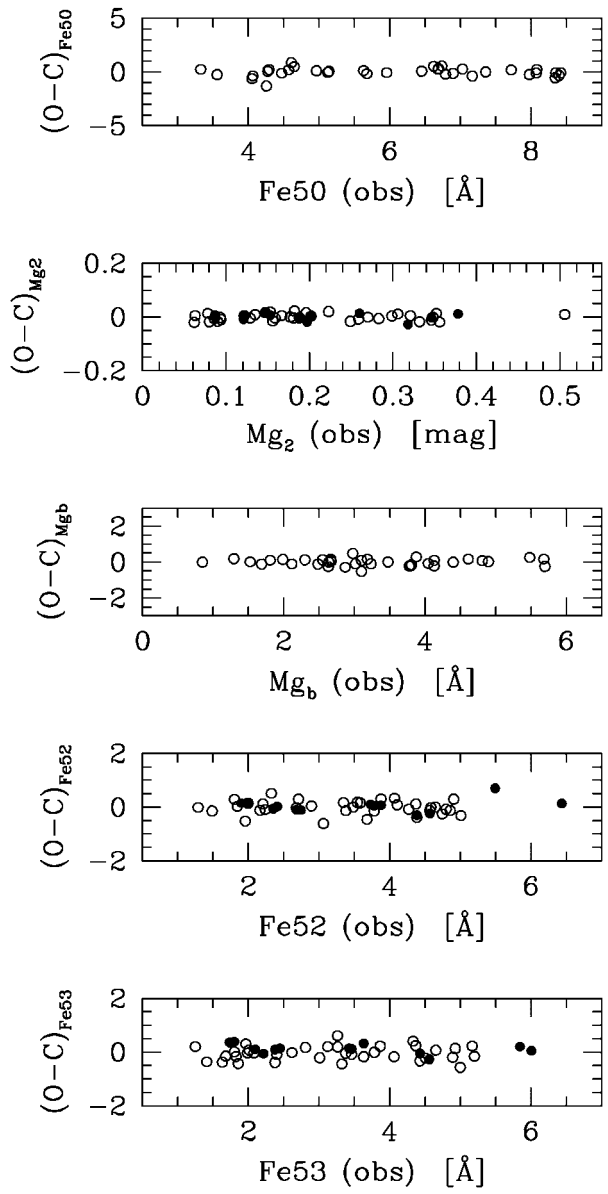

FIG. 1.—Index calibration to the standard Lick system. Residuals for the 36 primary calibrators (of luminosity classes III, IV, and V) in common with W94 (*open circles*) and a "check sample" of 13 stars in common with B92 and B94 (*filled circles*) are displayed, after application of eq. (4). Point scatter is $\sigma(\mathrm{Fe50}) = \pm 0.39$ Å, $\sigma(\mathrm{Mg_2}) = \pm 0.012$ mag, $\sigma(\mathrm{Mg}\ b) = \pm 0.19$ Å, $\sigma(\mathrm{Fe52}) = \pm 0.24$ Å, and $\sigma(\mathrm{Fe53}) = \pm 0.25$ Å. These values are comparable with the internal uncertainty in the observations, confirming the reliability of the calibration procedure.

In our analysis we had to face of course some intervening limitations of the Chavez et al. (1997) database, based on Kurucz (1993) models, at lower temperature and gravity. While, on the one hand, the plane-parallel layer approximation is no longer valid in the model atmosphere for low-gravity stars

($\log g < 1.5$ dex), the incomplete sampling of the molecular contribution leads, on the other hand, to a poor representation of the SED in the case of stars cooler than 4000 K.

In addition, when dealing with mid-resolution spectra, our models showed that some unavoidable degeneracy in the allowed range of the atmosphere physical parameters is present, and statistically equivalent best fits to the observations may be provided by theoretical spectra with slightly different combinations of the distinctive parameters.

For example, we verified that the effect of any change in the effective temperature of a star can be compensated by a combined change of gravity and metallicity such as

$$\Delta \log g/\Delta T_{\rm eff} = 1.3(1000/T_{\rm eff})^4 \text{ dex K}^{-1} \quad (9)$$

and

$$\Delta[\text{Fe/H}]/\Delta T_{\rm eff} = 7 \times 10^{-4} \text{ dex K}^{-1}. \quad (10)$$

Therefore, a warmer fitting temperature would accordingly imply a higher surface gravity and metallicity.

The [Fe/H] versus $T_{\rm eff}$ dependence increases even more in the case where we set gravity in the fitting synthetic spectra. Our tests show that

$$\Delta[\text{Fe/H}]/\Delta T_{\rm eff} = 0.2(1000/T_{\rm eff})^3 \text{ dex K}^{-1}. \quad (11)$$

On the other hand, an opposite trend would result between gravity and metallicity in the case where we could fix the fitting temperature:

$$\Delta[\text{Fe/H}]/\Delta \log g = -0.35; \quad (12)$$

that is, a higher metal abundance is required to balance absorption features that are "too shallow" in a spectrum in the case of a lower surface gravity.

While therefore our mid-resolution observations alone prevented an unequivocal fit to the data, they allowed us, however, to discriminate among different high-resolution parameter sets and single out the best one for each star.

A total of 64 out of 91 stars in the extended sample turned out to be consistent with a metal abundance [Fe/H] ≥ 0.1 dex, suggesting that about 2/3 of the whole sample of 139 stars actually consists of bona fide SMR stars.

As for the observed spectra, narrowband spectral indices have also been computed for the corresponding set of synthetic spectra and transformed to the Lick system by means of the empirical calibration of equation (4).

In Figure 2 we report the final residuals for the corresponding subsample of index calibrators with the available fiducial model (the $(O - C)$ residual distribution is now in the sense [synthetic − standard]). This consists of 25 primary reference stars in the W94 sample and nine stars from the B92 and B94 list.

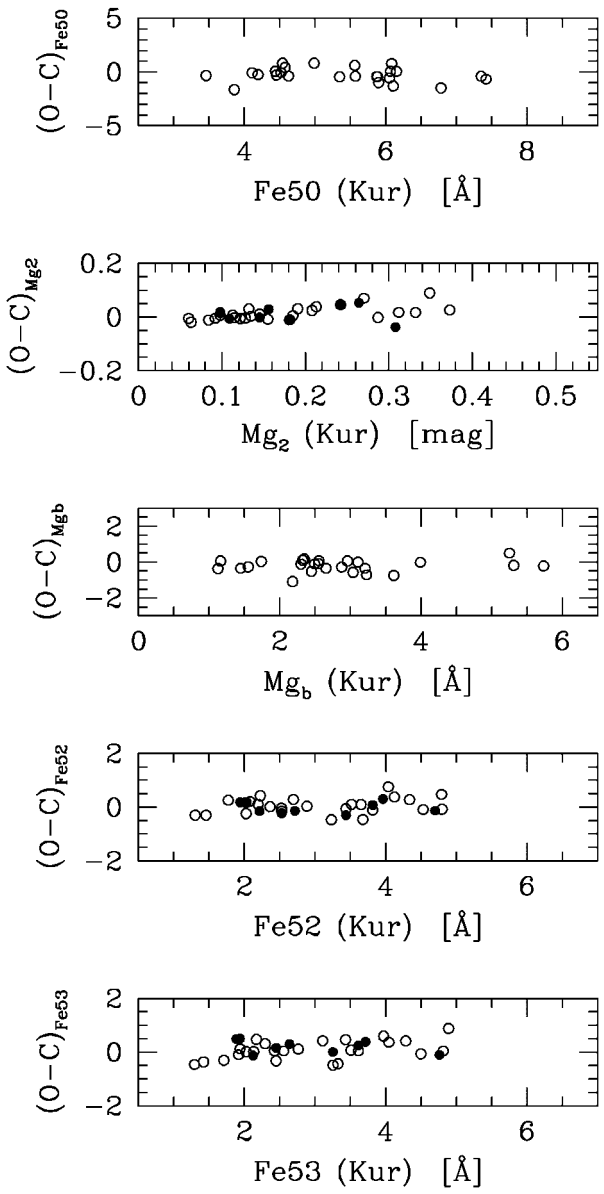

FIG. 2.—Index calibration to the standard Lick system, after eq. (4), for the fiducial model atmospheres of the 25 primary calibrators in common with W94 (*open circles*) and the nine stars from B92 and B94 (*filled circles*). The $(O - C)$ residuals are in the sense [synthetic − standard]. Point scatter is σ(Fe50) = ±0.70 Å, $\sigma(\text{Mg}_2)$ = ±0.029 mag, σ(Mg *b*) = ±0.40 Å, σ(Fe52) = ±0.27 Å, and σ(Fe53) = ±0.34 Å. These higher values, compared with those of the observations (see Fig. 1), give a measure of the residual variance of the theoretical models due to the intrinsic limitation of the input physics.

Point scatter in Figure 2 is slightly higher compared with the observations (especially for the magnesium indices and Fe50). This can be regarded as a measure of the "internal uncertainty" in the theoretical models due to the intrinsic lim-

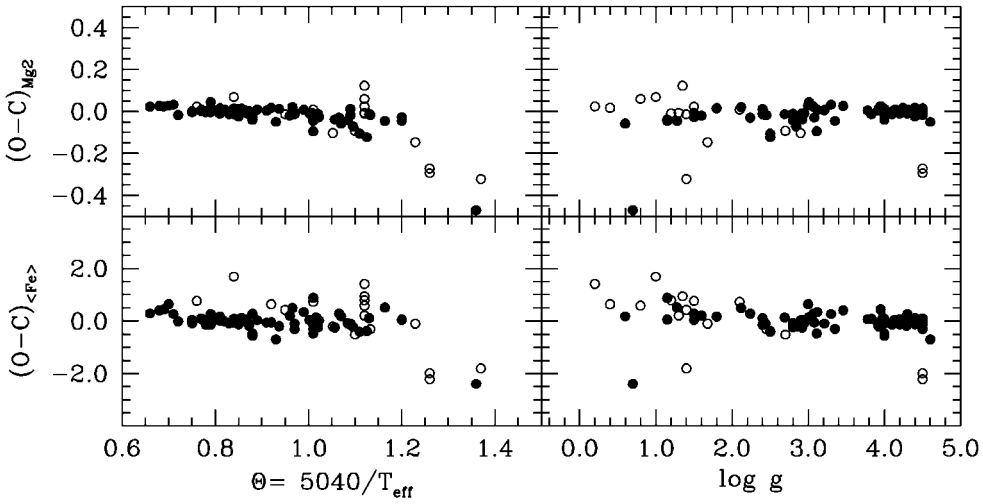

FIG. 3.—The ($O - C$) index residuals (in the sense [Observed − Synthetic]) for Mg_2 and combined iron index ⟨Fe⟩ are displayed vs. atmosphere fiducial parameters $\Theta = 5040/T_{\rm eff}$ and surface gravity. Filled circles mark the fair sample of 73 stars, while open circles include the supplementary 18 stars with less confident atmosphere match. As expected, the four coolest stars in the sample ($T_{\rm eff} \leq 4000$ K) are poorly matched by the models while the remaining point distribution is consistent with a zero-average residual. These four outliers will not enter any further analysis.

itation of the input physics:

$$\begin{aligned}
\sigma(\text{Fe50}) &= \pm 0.70 \text{ Å} \quad 25 \text{ stars},\\
\sigma(\text{Mg}_2) &= \pm 0.029 \text{ mag} \quad 34 \text{ stars},\\
\sigma(\text{Mg } b) &= \pm 0.40 \text{ Å} \quad 25 \text{ stars},\\
\sigma(\text{Fe52}) &= \pm 0.27 \text{ Å} \quad 34 \text{ stars},\\
\sigma(\text{Fe53}) &= \pm 0.34 \text{ Å} \quad 34 \text{ stars}. \qquad (13)
\end{aligned}$$

3.1. Index Calibration and Atmosphere Parameters

A more direct hint of the accuracy of the atmosphere fundamental parameters, at least for the 91 stars in our extended sample, can be found by comparing the ($O - C$) distribution (in the sense [observed − synthetic]) versus the fiducial set of temperature, gravity, and metallicity. We especially focused on the Mg_2 index and the "combined" Fe index defined as ⟨Fe⟩ = (Fe52 + Fe53)/2 (Faber et al. 1985).

The ($O - C$) trend versus surface gravity and temperature parameter $\Theta = 5040/T_{\rm eff}$ is studied in Figure 3. While a better match is achieved for the fair sample (*filled circles*), an increasing fraction of deviating points appears among cool (super-) giant stars (see open circle distribution).

In both the Mg_2 and the ⟨Fe⟩ plots, four outliers, namely, stars HD 36389 (spectral type M2 Iab), HD 88230 (K8 V), HD 146051 (M0.5 III), and HD 157881 (K7 V), display a very negative ($O - C$). These are the four coolest stars in our sample, with $T_{\rm eff} \leq 4000$ K. As discussed in B92 and Chavez, Malagnini, & Morossi (1996), most of this discrepancy arises from poor knowledge of molecular line opacities at cooler temperatures. This makes the atmosphere pseudocontinuum at 5000–5300 Å higher and the relevant indices stronger. These four stars will be excluded from further analyses, and we are therefore left with 72 stars for the fair sample and 87 stars for the extended sample.

The resulting metallicity scale, as from the fiducial atmosphere parameters of Paper I, is reported in Figure 4. As for Figure 3, the ($O - C$) distribution versus [Fe/H] does not show any significant trend and is consistent in any case with a zero average. At least six stars can be confidently recognized on the plot with a metallicity in excess of [Fe/H] > +0.35 dex. Some of these SMR candidates have been discussed in detail in Paper I.

3.2. Magnesium versus Iron Relative Abundance

A study of the Mg_2 and ⟨Fe⟩ residuals could also provide important information about the Mg versus Fe relative abundance. Because Kurucz model atmospheres and Chavez et al. (1997) synthetic spectra assume a solar chemical partition (so that [Mg/Fe] = 0.0, by definition), any systematic deviation in the index residuals could track, on the average, a nonstandard chemical mix for real stars.

Two opposite trends in the ($O - C$) distribution might be envisaged, in this respect, depending on whether they are induced by a biased set of atmosphere parameters or rather by a nonsolar abundance partition for [Mg/Fe]. In the first case, a mismatch of $T_{\rm eff}$ and/or $\log g$ would be reflected in a nominal metallicity shift (as a result of eqs. [10], [11], and [12]) and therefore in a *correlated* trend of Mg_2 and ⟨Fe⟩ ($O - C$) resid-

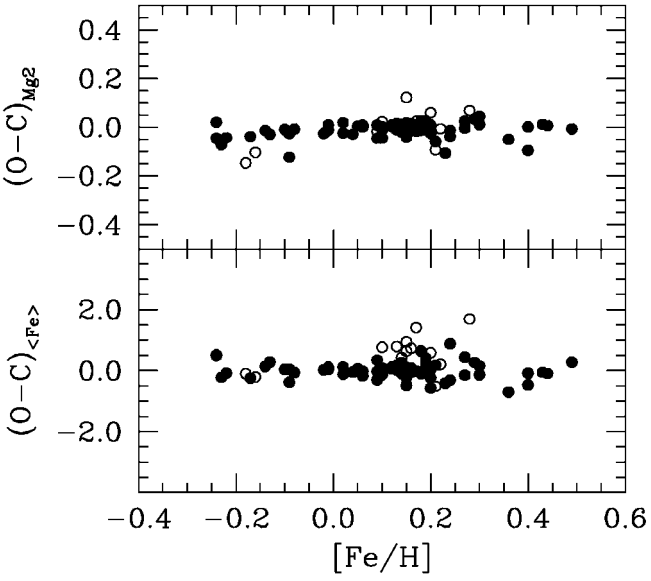

FIG. 4.—The metallicity scale is explored vs. $(O - C)$ index residuals (in the sense [observed − synthetic]) as in Fig. 3. No $(O - C)$ trend is found vs. [Fe/H], with index residual distribution consistent with a zero average. At least six stars can be confidently recognized with [Fe/H] in excess of +0.35 dex.

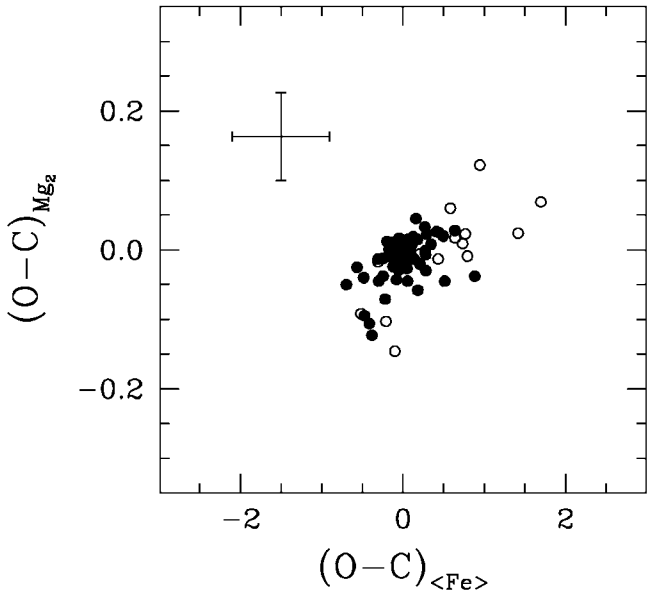

FIG. 5.—Mg_2 and ⟨Fe⟩ index residuals between observations and fiducial synthetic spectra are displayed for the fair (*filled circles*) and the extended (*open circles*) samples. The typical 2 σ error box of individual observations is displayed in the upper left of the figure. The lack of any clear *anticorrelated* trend between the $(O - C)$ residuals indicates, on the average, a solar [Mg/Fe] relative abundance. See text for discussion.

uals. On the other hand, any *intrinsic* change of the [Mg/Fe] relative abundance would induce *anticorrelated* $(O - C)$ residuals for the two indices.

As far as the fair sample is accounted for in our analysis (see filled circle distribution in Fig. 5), no statistically significant trend between Mg and Fe indices is evident within a 2 σ confidence level. As expected, most of the deviating points in the figure belong to the extended sample, and the correlated distribution in the latter case is therefore induced as a result of the less accurate atmosphere fit.

In conclusion, we have therefore no evident sign of a systematic trend in the [Mg/Fe] relative abundance, and a standard chemical partition seems consistent with the data.

4. COMPARISON WITH INDEX FITTING FUNCTIONS

Lick narrowband indices have proven to be a useful diagnostic tool not only for probing atmosphere physical properties in individual stars but also for studying stellar populations as a whole (Buzzoni 1995, 1996; Worthey, Faber, & Gonzalez 1992; Worthey, Trager, & Faber 1996).

In particular, population synthesis models have made extensive use of the "fitting function" technique to compute integrated indices for theoretical stellar systems.

This procedure relies on analytical fits of the index strength versus stellar fundamental parameters (namely, $\log T_{\rm eff}$, $\log g$, and [Fe/H]) across the H-R diagram and allows spectroscopic features to be synthesized for stellar aggregates even by means of low-resolution models of the integrated SED.

For example, if an index I can be defined for individual stars in a magnitude scale as in equation (2), then by summing up on the whole stellar population, we have

$$I_{\rm tot} = -2.5 \log \left[\frac{\sum_* f_c(i) \times 10^{-0.4 I(i)}}{\sum_* f_c(i)} \right]. \qquad (14)$$

If the dex term in the right-hand upper sum can be evaluated analytically for each composing star, then the integrated index simply follows in terms of the total continuum luminosity of the whole population, $L_{\rm tot} = \sum_* f_c(i)$ (see B92 for a first application of this technique to the Mg_2 synthesis).

Analytical fitting functions for iron and magnesium indices have been provided by B92, B94, and Gorgas et al. (1993). The latter set of equations was then revised by W94 including a larger number of features in the optical wavelength range and calibrating versus effective temperature.

It could be useful to test the self-consistency of these functions also in the SMR regime in order to secure their application to the synthesis of metal-rich stellar environments, as in the case of the Galaxy bulge or external early-type galaxies.

A first check in this sense can be done by studying the index residuals of our observations with respect to the B92, B94, and

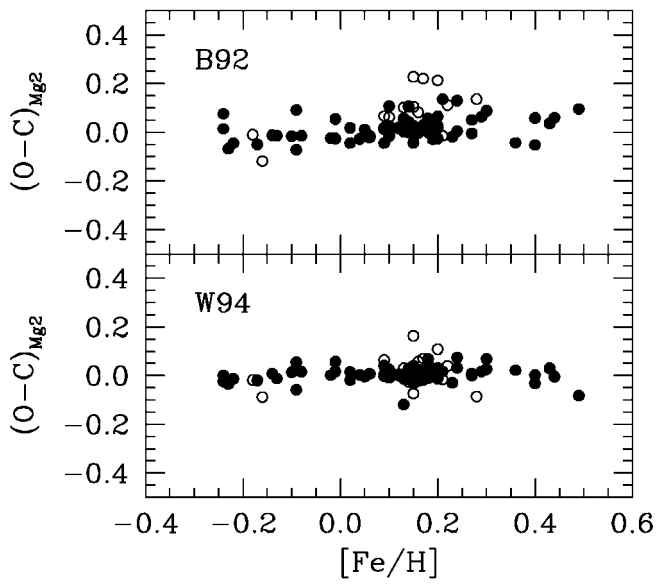

FIG. 6.—Mg_2 index residuals (in the sense [observed − computed]) with respect to B92 and W94 fitting functions vs. metallicity for the fair (*filled circles*) and the extended (*open circles*) samples. Both $(O - C)$ distributions are consistent with a zero average. Point spread for the fair sample across the B92 fitting function is $\sigma(Mg_2) = \pm 0.049$ mag, and $\sigma(Mg_2) = \pm 0.031$ mag with respect to W94.

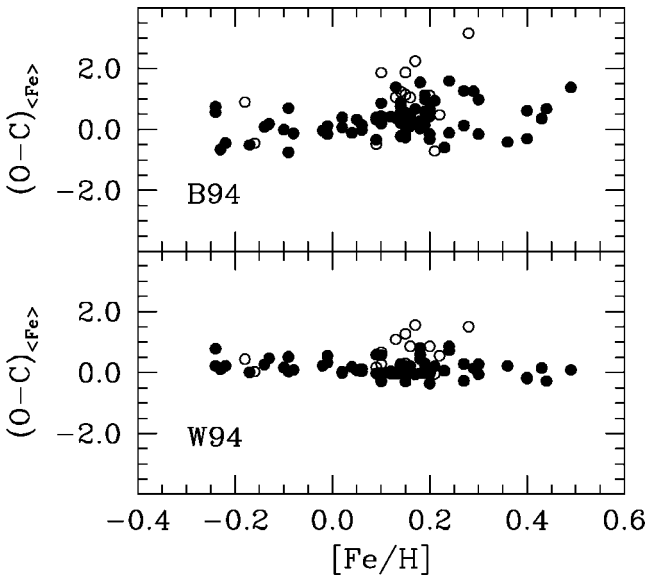

FIG. 7.—Same as Fig. 6 but for the combined Fe index $\langle Fe\rangle = (Fe52 + Fe53)/2$. Point spread of the fair sample (*filled circles*) with respect to the zero-average $(O - C)$ is $\sigma(\langle Fe\rangle) = \pm 0.61$ Å compared with B94 and $\sigma(\langle Fe\rangle) = \pm 0.30$ Å with respect to W94.

W94 sets of fitting functions. Figure 6 summarizes our results for Mg_2.

Both $(O - C)$ distributions in the figure are consistent with a zero average residual, confirming that the two sets of equations properly account for high-metallicity stars. The W94 fitting function is slightly more accurate than the B92 one [the point spread for the fair sample is $\sigma(Mg_2) = \pm 0.031$ mag versus $\sigma(Mg_2) = \pm 0.049$ mag for the latter case] but at the cost of a more elaborate analytical fit consisting of four different polynomials along the temperature range of stars.[4]

A similar behavior is also found for the $\langle Fe\rangle$ index (see Fig. 7), with $\sigma(\langle Fe\rangle) = \pm 0.61$ Å with respect to B94 and $\sigma(\langle Fe\rangle) = \pm 0.30$ Å with respect to the W94 three-branch fit. We verified that the skewed positive residuals with respect to B94, evident from the figure, mostly come from the warmer stars in the sample ($T_{\rm eff} \gtrsim 6700$ K), for which the fitting function predicts a vanishing Fe52 index.

The Fe50 and Mg *b* features have been accounted for only by W94. Fitting function predictions are compared with observations in Figure 8. The data seem more poorly matched, compared with Mg_2 and $\langle Fe\rangle$, with a more important $(O - C)$ spread [$\sigma(Fe50) = \pm 0.95$ Å, and $\sigma(Mg\ b) = \pm 0.83$ Å for the fair sample] and a nonzero $(O - C)$ average.

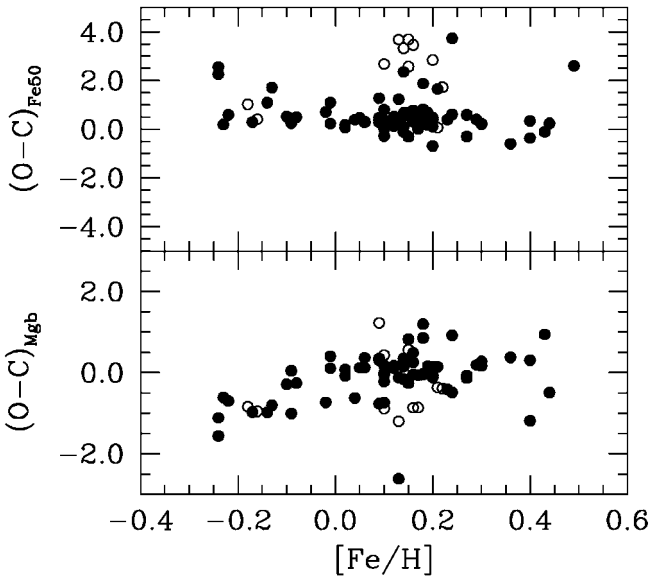

FIG. 8.—Same as Fig. 6 but for the Fe50 and Mg *b* indices. The $(O - C)$ residuals are computed with respect to the W94 fitting functions. Point spread for the fair sample (*filled circles*) with respect to the zero-average $(O - C)$ is $\sigma(Fe50) = \pm 0.95$ Å, and $\sigma(Mg\ b) = \pm 0.83$ Å. A trend with [Fe/H] (opposite for Fe50 and Mg *b*) appears in the data.

[4] Quite importantly, note that an incorrect version of one of the four polynomial branches is given in the Worthey et al. (1994) Table 3. The claimed log Θ dependence of the fit should in fact be read as a simple Θ dependence. The same problem also affects all the other indices discussed in this work.

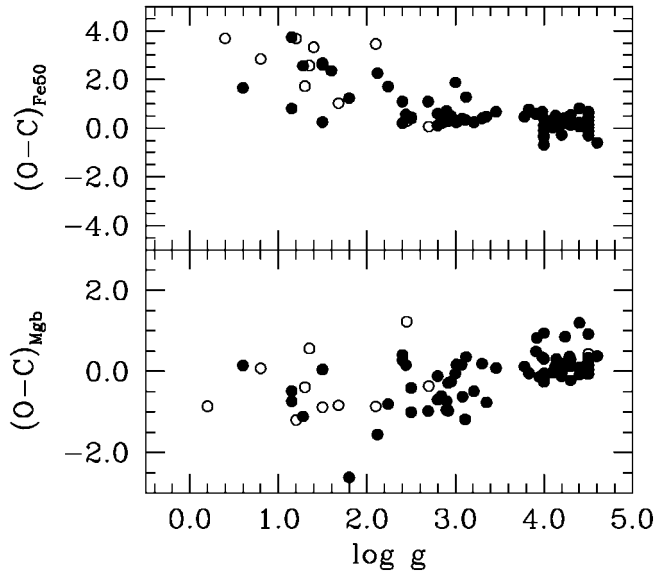

FIG. 9.—Fe50 and Mg *b* ($O - C$) residuals as from Fig. 8 vs. stellar gravity. The drift in the data distribution indicates that log *g* dependence is not fully accounted for by the W94 fitting functions. The residual variance is directly reflected in the poorer match to the observations in Fig. 8.

If we explore the ($O - C$) distribution versus stellar surface gravity (see Fig. 9), we find that the drift of the data is increased, confirming that log *g* dependence has not been fully accounted for by the W94 fitting functions. This residual variance is expected to induce a biased measure of the integrated Fe50 and Mg *b* as far as population synthesis models are computed relying on the W94 theoretical framework. Special caution should therefore be recommended in the synthesis of these indices.

4.1. Fitting Functions and Index Fit

Although each of the B92, B94, and W94 fitting functions ensures a convenient representation of the Mg_2 and $\langle Fe \rangle$ indices in the metallicity range of our observations, it is however worthwhile to briefly discuss here a possible important bias introduced by any unwarranted use of the fitting function technique to reproduce stellar indices.

The problem could be of paramount importance in the case of population synthesis models, where fitting functions are used to make a systematic prediction of index behavior across the whole H-R diagram and often beyond the boundary limits of the formal fitting domain.

An instructive example in this sense is given in Figure 10, where we compare the Mg_2 distribution of our stellar sample with the B92 and W94 analytical output. In order to span the whole range of temperatures, to our stars we also added (in both panels of Fig. 10) the Mg_2 measurements of eight Gliese red dwarfs from B92 and 10 M dwarfs from the Gorgas et al. (1993) sample with 3000 K $< T_{\rm eff} <$ 4300 K, according to the ($V - K$) versus $T_{\rm eff}$ calibration of W94 (see Table 6 therein).

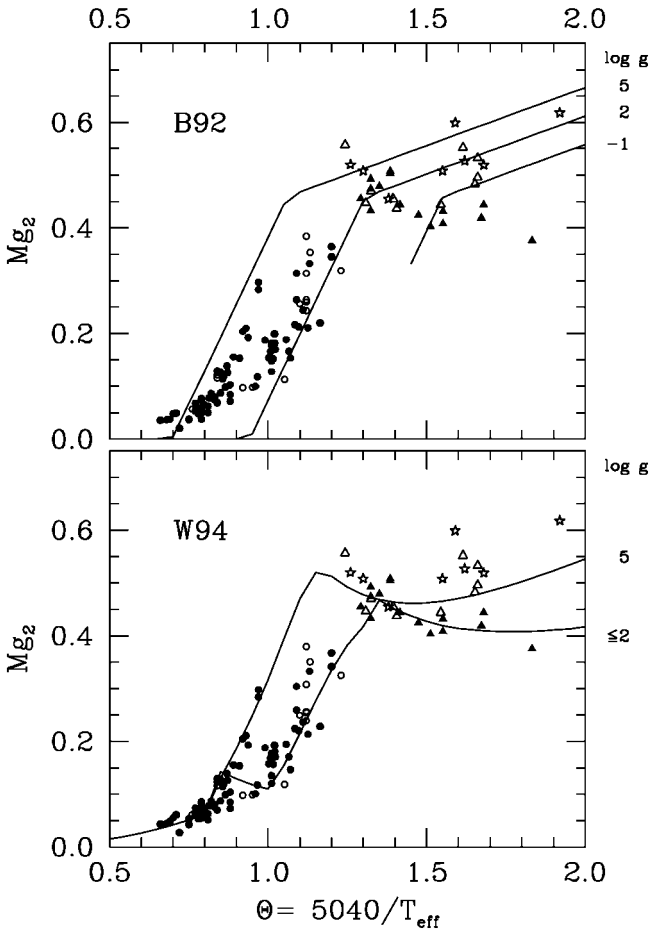

FIG. 10.—Mg_2 data distribution for the fair (*filled circles*) and extended (*open circles*) samples vs. B92 and W94 fitting-function predictions (*solid lines*). To ease comparison, observations have been corrected to [Fe/H] = 0 by subtracting the corresponding [Fe/H] polynomial term of each fitting set. In order to span the whole range of temperature, Mg_2 measurements of eight Gliese red dwarfs from B92 (*stars*) have also been added in both panels together with 10 M dwarfs from the Gorgas et al. (1993) sample (*open triangles*). The low-gravity range is also spanned by a set of 16 field M giants with $T_{\rm eff} < 3900$ K, from W94 (*filled triangles*). The B92 and W94 fitting functions have been computed for log g = 5.0,2.0, and −1.0 dex, as labeled in each panel. Below 3900 K the W94 fit is insensitive to stellar gravity, so the log g = 2 and −1 curves merge. A solar metallicity is assumed throughout in the models.

A set of 16 field M giants with $T_{\rm eff} < 3900$ K, from Table A2C of W94, is also included in the figure to span low-gravity stars.

To ease comparison, our observations have been corrected for metallicity and reconducted to [Fe/H] = 0 by subtracting the [Fe/H] polynomial term according to the different fitting sets. In each panel of Figure 10, three theoretical loci are computed for log g = 5.0, 2.0, and −1.0 dex at solar metallicity.

While both fitting sets properly comprise our data distribution (thus confirming the adequacy of the fit, as we discussed in the previous section), it is however evident that a different trend for the Mg_2 index is predicted at low temperature.

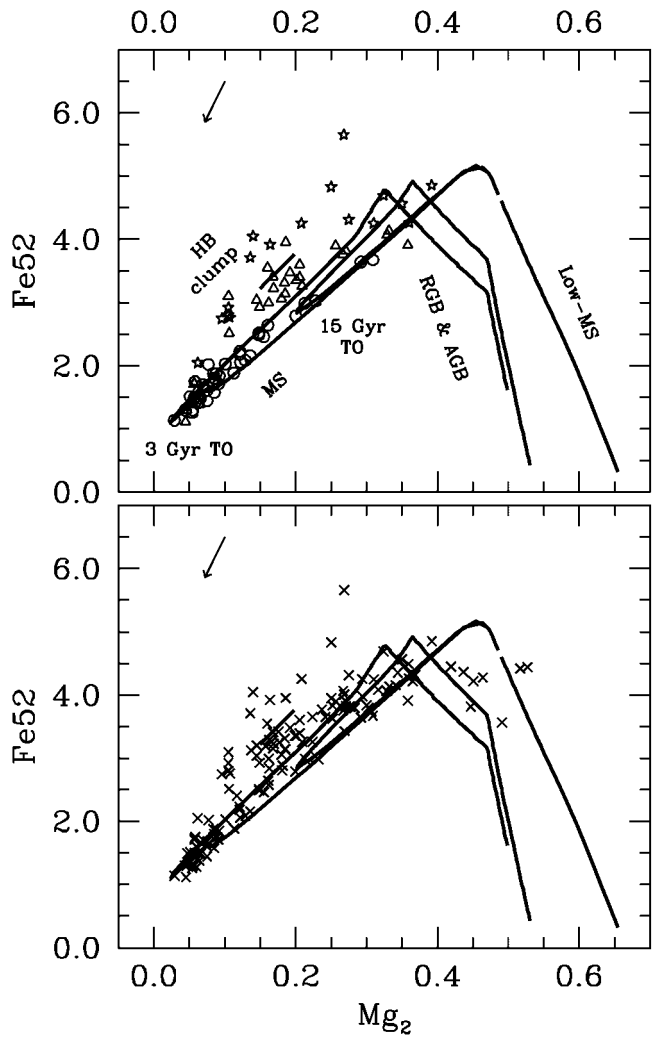

FIG. 11.—Mg_2 vs. Fe52 distribution for (*upper panel*) the 87 stars with fiducial atmosphere parameters in the extended sample and for (*lower panel*) the global observed sample of 139 stars. Stars in the upper panel are marked according to their surface gravity (*stars*: $\log g < 2.0$; *open triangles*: $2.00 \leq \log g \leq 3.5$; *open circles*: $\log g > 3.5$). The theoretical locus for 3 and 15 Gyr old simple stellar populations with [Fe/H] $= +0.2$ from Buzzoni (1989) is superposed on the data, and main evolutionary phases are labeled (main sequence [MS], turnoff point [TO], red giant branch [RGB], asymptotic giant branch [AGB], and horizontal branch [HB]). The vector top left in each panel is the expected variation in the observed indices for a change in [Fe/H] of -0.5 dex.

Compared with W94, for $\Theta \gtrsim 1.3$ ($T_{\rm eff} \lesssim 3900$ K) the B92 fitting function shows a steeper increase in the Mg index. This better matches the red dwarf data, although some marginal evidence exists for an overestimate of the M giants. On the other hand, the W94 fit predicts slightly lower values for Mg_2 throughout in the low-temperature range and partially misses the red dwarf data. Moreover, an artificial glitch is evident in one of the fitting branches of the W94 set at about $\Theta = 0.8$–1.0 for $\log g = 2$.

Such different behavior in the H-R diagram description is directly reflected in the theoretical output when integrated indices for population synthesis models are computed. This explains, for instance, the systematically lower values for Mg_2 in the Worthey (1994) simple stellar population models compared with B92.

5. THE Mg_2 VERSUS Fe52 DIAGNOSTICS

Given a selective dependence on the atmosphere fundamental parameters, a combined study of the Mg and Fe Lick indices could give direct hints on the distinctive parameters of stars.

A two-index plot, like in Figure 11, summarizes in facts most of the relevant features of a CM diagram but with the major advantage of being both reddening free and distance independent and points therefore to the intrinsic properties of stars.

In the upper panel of Figure 11 we study the fair sample distribution in the Mg_2 versus Fe52 index domain with two [Fe/H] $= +0.22$ dex isochrones of 3 and 15 Gyr from the Buzzoni (1989) synthesis code. Surface gravity of stars in our sample has been singled out for a better comparison with the models, while the main evolutionary phases for both isochrones have been labeled on the plot.

A quite good agreement exists between high-gravity stars ($\log g > 3.5$ dex) and the main-sequence locus, confirming that objects as young as 3 Gyr are present in our sample. This makes an Mg_2/Fe52 plot a simple and very powerful tool for estimating ages of stellar populations.

Stars of intermediate gravity ($2.0 \geq \log g \geq 3.5$) consistently "bunch" around the expected locus for the core helium-burning stars (both the horizontal branch phase of low-mass stars and the first blue loop of high-mass objects), while a lack of objects close to the tip of the red and asymptotic giant branches (i.e., for a vanishing value of Fe52 with $Mg_2 \gtrsim 0.4$ in the plot) seems to indicate a prevailing presence in our sample of high-mass stars ($M > 2\ M_{\odot}$) developing a non–He-degenerate red giant phase.

It is a pleasure to thank Guy Worthey, the referee of this paper, for his valuable input and important suggestions. This project received partial financial support from the Italian MURST under COFIN'98 02-013, COFIN'00 02-016, and 60% grants and from the Mexican CONACyT via grant 28506-E.

REFERENCES

Brodie, J. P., & Huchra, J. P. 1990, ApJ, 362, 503
Buzzoni, A. 1989, ApJS, 71, 817
———. 1995, ApJS, 98, 69
———. 1996, in ASP Conf. Ser. 86, Fresh Views of Elliptical Galaxies, ed. A. Buzzoni, A. Renzini, & A. Serrano (San Francisco: ASP), 189
Buzzoni, A., Gariboldi, G., & Mantegazza, L. 1992, AJ, 103, 1814 (B92)
Buzzoni, A., Mantegazza, L., & Gariboldi, G. 1994, AJ, 107, 513 (B94)
Cayrel de Strobel, G., Soubiran, C., Friel, E. D., Ralite, N., & François, P. 1997, A&AS, 124, 299
Chavez, M., Malagnini, M. L., & Morossi, C. 1996, ApJ, 471, 726
———. 1997, A&AS, 126, 267
Faber, S. M., Burstein, D., & Dressler, A. 1977, AJ, 82, 941
Faber, S. M., Friel, E. D., Burstein, D., & Gaskell, C. M. 1985, ApJS, 57, 711
Frogel, J. A. 1999, Ap&SS, 265, 303
Gorgas, J., Faber, S. M., Burstein, D., Gonzalez, J. J., Courteau, S., & Prosser, C. 1993, ApJS, 86, 153
Kurucz, R. L. 1993, CD-ROM 13, ATLAS9 Stellar Atmosphere Programs and 2 km s^{-1} Grid (Cambridge: SAO)
Malagnini, M. L., Morossi, C., Buzzoni, A., & Chavez, M. 2000, PASP, 112, 1455 (Paper I)
McWilliam, A. 1997, ARA&A, 35, 503
Smith, G., & Ruck, M. J. 2000, A&A, 356, 570
Spinrad, H., & Taylor, B. J. 1969, ApJ, 157, 1279
Taylor, B. J. 1991, ApJS, 76, 715
———. 1999, A&A, 344, 655
Worthey, G. 1994, ApJS, 95, 107
Worthey, G., Faber, S. M., & Gonzalez, J. J. 1992, ApJ, 398, 69
Worthey, G., Faber, S. M., Gonzalez, J. J., & Burstein, D. 1994, ApJS, 94, 687 (W94)
Worthey, G., Trager, S. C., & Faber, S. M. 1996, in ASP Conf. Ser. 86, Fresh Views of Elliptical Galaxies, ed. A. Buzzoni, A. Renzini, & A. Serrano (San Francisco: ASP), 203